RSC Advances

PAPER

View Article Online
View Journal | View Issue



Cite this: *RSC Adv.*, 2017, **7**, 25455

# Synthesis of four-angle star-like CoAl-MMO/$BiVO_4$ p–n heterojunction and its application in photocatalytic desulfurization

Limin Yun,[a] Zhanxu Yang,*[a] Zong-Bao Yu,[a] Tianfeng Cai,[a] Yue Li,[b] Changyou Guo,[c] Chengyuan Qi[a] and Tieqiang Ren[a]

Received 13th March 2017
Accepted 25th April 2017

DOI: 10.1039/c7ra03012f

rsc.li/rsc-advances

A four-angle star-like Co–Al mixed metal oxide (CoAl-MMO)/$BiVO_4$ heterojunction has been synthesized *via* a hydrothermal method and following sintering. The CoAl-MMO/$BiVO_4$ is derived from CoAl-LDHs/$BiVO_4$, in which CoAl-LDHs leads to a distribution of amorphous CoAl-MMO. The CoAl-MMO loading on $BiVO_4$ greatly enhances visible light absorption, improves charge separation by band offset charge transfer, and makes flat band potential more negative. The three effects together result in excellent photocatalytic activity. Under visible light irradiation, desulfurization efficiency of thiophene has achieved up to 98.58% on CoAl-MMO/$BiVO_4$ with molar ratio of 0.3 : 5.



## Introduction

Organic sulfur from petroleum is a major contributor to environmental pollution. Nowadays, the most widely employed method to remove thiophenic compounds in fuel are hydrodesulfurization (HDS)[1] and adsorption desulfurization.[2] Both of the processes need hydrogen, relatively high-pressure conditions and high energy consumption for deep desulfurization. Therefore, the development of desulfurization process with low energy consumption, mild operating conditions and environmental friendliness has become the research focus.[3]

Photocatalytic desulfurization technology has attracted much attention, because it can provide a cleaner and more environmental friendly way to realize desulfurization. $TiO_2$-based photocatalyst has been widely studied and used in photocatalytic oxidative desulfurization.[4] But since its band gap is 3.2 eV, it can only absorb UV light, which limits its application.[5] Therefore, the development of photocatalysts with visible light response has become a research hotspot. Bismuth vanadate ($BiVO_4$, n-type semiconductor), with a band gap of 2.4 eV, has attracted much attention because it shows activation under visible light irradiation.[6–10] However, the photocatalytic activity of pure $BiVO_4$ is always low because of the rapid recombination of carriers (electrons and holes). To overcome these drawbacks, strategy of heterogeneous structure construction has been developed,[11–14] to spatially separate photogenerated carriers by band offset. Besides, one widely common strategy is to combine $BiVO_4$ with other noble metal or noble metal oxides,[15,16] such as Pt, Ag, $RuO_2$. For example, Lin *et al.*[17] reported a visible-light responsive photocatalyst $BiVO_4$ co-loaded with Pt and $RuO_2$ co-catalysts, which photocatalytically oxidized thiophene to $SO_3$ and achieved over 99% of thiophene conversion. Gao *et al.*[18] synthesized Ag–$BiVO_4$ photocatalysts *via* hydrothemal method and photocatalytic desulfurization efficiency under visible light irradiation at pH = 7 could be up to 95%. Although the desulfurization efficiency of the above photocatalyst is high, the cost of cocatalysts using noble metal or noble metal oxides is expensive. It is necessary to develop low-cost cocatalysts to combine with $BiVO_4$ to achieve efficient desulfurization.

Herein we report the photocatalytic oxidation of thiophene by Co–Al mixed metal oxide (CoAl-MMO) loaded $BiVO_4$. However, investigation indicates that CoAl-MMO does not act as cocatalyst of $BiVO_4$, but gets three unprecedented effects. The CoAl-MMO loading enhances visible light absorption, improves charge separation by band offset charge transfer, and makes flat band potential more negative. Combination of these effects largely enhances photocatalytic efficiency of thiophene oxidation. The CoAl-MMO derives from a Co–Al-layered double hydroxide (CoAl-LDH) precursor.[19,20] Since LDH has a uniform distribution of metal cations on the atomic level, sintering leads to CoAl-MMO with a uniform distribution of cobalt and aluminum.[21] It notes that band gap of $CoAl_2O_4$ (ref. 22) is narrow while that of $Al_2O_3$ is wide,[23] but neither has been found from our sample by X-ray diffraction (XRD). Besides XRD, samples were characterized by scanning electron microscopy (SEM) and transmission electron microscopy (TEM), ultraviolet-visible diffusive reflectance spectroscopy (UV-vis DRS) and photoluminescence (PL) spectra. The desulfurization activity has been explored under visible-light.

[a]*College of Chemistry, Chemical Engineering and Environment Engineering, Liaoning Shihua University, Fushun, Liaoning 113001, P. R. China. E-mail: zhanxuy@126.com*
[b]*School of Foreign Languages, Liaoning Shihua University, Fushun, Liaoning 113001, P. R. China*
[c]*SINOPEC Fushun Research Institute of Petroleum and Petrochemicals, Fushun 113001, China*

## Experiment

### Chemicals

All the reagents were analytical grade and used without any further purification.

### Preparation of $BiVO_4$ and CoAl-MMO/$BiVO_4$ samples

In a typical synthesis, under stirring conditions, 0.17 mmol P123 (analysis) and 5 mmol $Bi(NO_3)_3 \cdot 5H_2O$ were dissolved in a mixed solution of 5 mL $HNO_3$ solution (3 mol $L^{-1}$) and 20 mL ethylene glycol solution to obtain solution A. 5 mmol $NH_4VO_3$ was dissolved in 20 mL deionized water with 70 °C to obtain solution B. Solution A and B at room temperature were stirred for 30 min each, then solution A was added to B dropwise. Then pH value was adjusted with $NH_3$ $H_2O$ (14 wt%) and was stirred for 60 min to obtain $BiVO_4$ precursor. A certain amount of $Co(NO_3)_2 \cdot 6H_2O$ and $Al(NO_3)_3 \cdot 9H_2O$ was dissolved in deionized water ($Co^{2+}/Al^{3+}$ molar ratio = 3 : 1), then a solution containing 1.0 mol $L^{-1}$ NaOH and 0.30 mol $L^{-1}$ $Na_2CO_3$ was added into it. Stirring for 60 min, Co–Al layered double hydroxide (CoAl-LDHs) precursor had been obtained. CoAl-LDHs precursor was added to $BiVO_4$ precursor, pH value was adjusted to 10 with NaOH (1.0 mol $L^{-1}$) solution and stirred for 60 another min. The mixed solution was transferred to a 100 mL Teflon lined stainless steel autoclave and hydrothermal treatment was conducted at 180 °C for 12 h. After that, the resulting CoAl-LDHs/$BiVO_4$ catalysts were washed with deionized water and absolute ethanol, dried at 80 °C for 3 h. Molar ratio of CoAl-LDHs/$BiVO_4$ for 0 : 5 ($BiVO_4$), 0.1 : 5, 0.3 : 5, 0.5 : 5 were controlled. Final products were obtained by sintering in a muffle furnace at a ramp of 1 °C $min^{-1}$ from 30 °C to 400 °C and maintaining for 4 h. The final products were noted as CoAl-MMO/$BiVO_4$.

### Characterizations

X-ray powder diffraction (XRD) measurements were performed on a Bruker D8 Advance diffractometer operated at 40 kV and 40 mA at the scanning range from 2 to 70 degree with Cu-Kα radiation (λ = 0.15406 nm). The particle morphologies of the products were observed by scanning electron microscopy (SEM) (Hitachi SU 8010) and by transmission electron microscopy (TEM) (JEM 2200FS). A Cary 5000 UV-vis spectrometer (Agilent Technologies) was used to obtain the reflectance spectra of the samples over a range of 400–800 nm. Electrochemical analysis was carried out with a standard three-electrode system with a Pt plate as the counter electrode, Hg/$Hg_2Cl_2$ (saturated with KCl) as a reference electrode, and ITO glass coated with the sample was used as the working electrode. A 0.5 M $Na_2SO_4$ solution was used as electrolyte. A 500 W Xe arc lamp (CHF-XM35-500W) was utilized as light source. Transient short-circuit photocurrent measurements and Mott–Schottky experiments with amplitude of 50 mV and a frequency of 1000 Hz were taken on a CHI660E workstation.

### Photocatalytic oxidative desulfurization tests

The photocatalytic oxidative desulfurization tests were carried out in a quartz tube reactor with a water condenser at atmospheric pressure and room temperature, using air and $H_2O_2$ (30%) as oxidants. The model oil, with sulfur content of 200 ppm is prepared by dissolving thiophene into *n*-octane. 50 mg photocatalyst and 50 mL model oil were added to the reactor. The suspension was stirred in dark for 30 min to obtain an adsorption–desorption equilibrium between the CoAl/$BiVO_4$ photocatalyst and model oil. Then, 0.128 mL $H_2O_2$ was added and the suspension was irradiated by a 500 W Xe arc lamp (CHF-XM35-500W), the airflow velocity was of 5 mL $min^{-1}$. Desulfurized oil was collected periodically and extracted with acetonitrile. Sulfur content was determined by a TSN-5000 series fluorescence nitrogen/sulfur analyzer (Jiangfen Electroanalytical Instrument Co., Ltd., China).

## Results and discussion

Fig. 1 shows XRD patterns of $BiVO_4$ and CoAl-MMO/$BiVO_4$ samples. The diffraction peaks at 2$\theta$ of 18.6°, 28.9°, 30.5°, 34.4°, 35.3°, 39.4°, 42.3°, 46.1°, 46.6°, 47.3°, 53.3°, 58.3°, and 59.9° can be observed, which index to monoclinic $BiVO_4$ (JCPDS no. 14-0688) and correspond to the crystalline planes of (101), (013), (112), (200), (020), (211), (105), (123), (204), (024), (301), (303) and (224).[24] It is clearly observed from the graph that as CoAl-MMO loading ratio increases, the intensity of CoAl-MMO/$BiVO_4$ samples becomes weaker; and no other peaks can be found in XRD patterns of CoAl-MMO/$BiVO_4$ catalysts, which may due to the amorphous characteristics of CoAl-MMO.

The morphology of samples has been characterized by SEM and TEM (Fig. 2). The morphology of $BiVO_4$ shows four angles with star-like and the particle size is uniform. After loaded with CoAl-MMO, the morphology becomes more regular. Low molar loading ratio makes the surface of CoAl-MMO/$BiVO_4$ particles look smooth, as molar loading ratio reaches 0.3 : 5, the surface become rough. And under magnified TEM many small particles on the surface can be observed (Fig. 2(d)). As red dashed line and red arrows point, CoAl-MMO nanoparticles are amorphous and dispersed on $BiVO_4$ surface. As shown in inset graph of Fig. 2(b) and (c), the thickness of CoAl-MMO/$BiVO_4$ with molar ratio 0.1 : 5 and 0.3 : 5 are about 750 nm and 1 μm, respectively, meaning that with the loading ratio increasing, more CoAl-

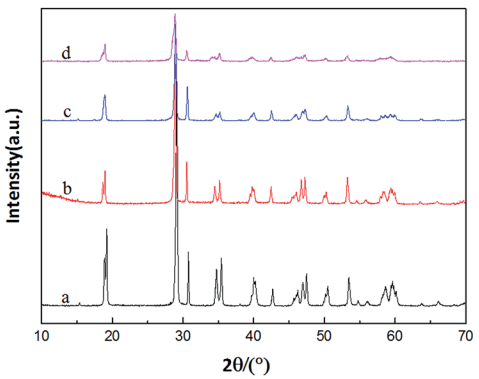


Fig. 1 XRD patterns of samples (a) $BiVO_4$ and CoAl-MMO/$BiVO_4$ with molar ratio (b) 0.1 : 5, (c) 0.3 : 5, (d) 0.5 : 5.

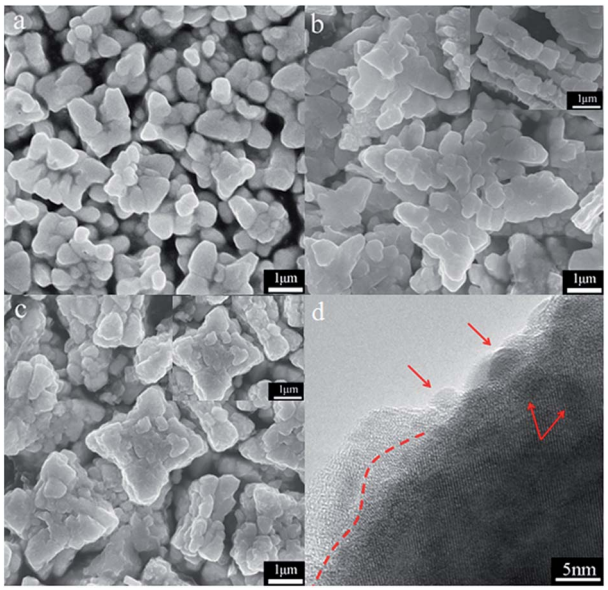


Fig. 2 SEM images of samples (a) $BiVO_4$ and CoAl-MMO/$BiVO_4$ with molar ratio (b) 0.1 : 5, (c) 0.3 : 5 and (d) TEM image of that with ratio of 0.3 : 5.

MMO formed on $BiVO_4$ surface and the particles become thicker. The particle size rises also, which may be due to CoAl-LDH playing a role of template.

Fig. 3(A) shows UV-vis diffuse reflectance spectra of $BiVO_4$ and CoAl-MMO/$BiVO_4$. $BiVO_4$ shows an absorption region between 200–530 nm, which covers both UV and partial visible light region. Interestingly, after loaded with CoAl-MMO the absorption region extends to 700 nm, which is throughout the UV to visible light region. For crystalline semiconductor, the optical absorption near the band edge follows the formula:[25]

$$\alpha h\nu = A(h\nu - E_g)^{n/2}$$

$\alpha$, $\nu$, $E_g$ and $A$ refer to coefficient, light frequency, band gap and a constant ($A = 1$), respectively. $n$ depends on the characteristics of the transition in a semiconductor, for direct transition, $n = 1$, for indirect transition $n = 4$. For $BiVO_4$, $n = 1$.[26] The plots of $(\alpha h\nu)^2$ *versus* photon energy ($h\nu$) is shown in the inset graph of Fig. 3(A), and the band gap of $BiVO_4$ and CoAl-MMO/$BiVO_4$ can be obtained by extroplating the curve to $\alpha = 0$. As a result, the band gaps CoAl-MMO/$BiVO_4$ with loading ratio of 0 : 5, 0.1 : 5, 0.3 : 5 and 0.5 : 5 obtained are 2.4 eV, 2.35 eV, 2.06 eV and 2.08 eV, respectively. Compared to $BiVO_4$, CoAl-MMO/$BiVO_4$ samples exhibit stronger absorption in the visible light range and narrower band gap. $BiVO_4$ is a n-type semiconductor[27] while $CoAl_2O_4$ p-type,[28] (although not detected by XRD but may exist as amorphous), a p–n heterojunction should have been formed at the interface of $CoAl_2O_4$ and $BiVO_4$ particles, which extends the absorption range and makes the band gap narrower. For sample with molar loading ratio of 0.3 : 5, these small particles on the surface leads to expanding of contact area and stable heterojunction structure. However, for sample 0.5 : 5, the absorption capacity become lower and the band gap slightly increases. It may be due to that some growing amount of CoAl-MMO particles are not well-loaded on the surface of $BiVO_4$, but just scatter around, which makes the heterojunction structure unstable and restrain the interface interaction between CoAl-MMO and $BiVO_4$.

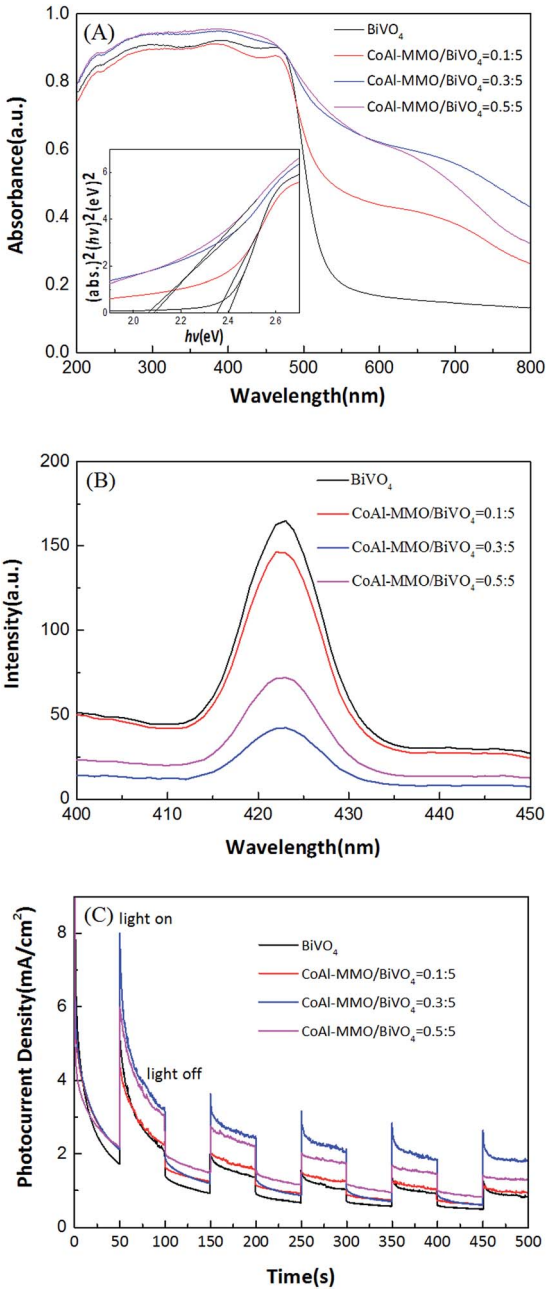


Fig. 3 (A) UV-vis diffuse reflectance spectra of $BiVO_4$ and CoAl-MMO/$BiVO_4$ samples, the inset shows plots of $(\alpha h\nu)^2$ *vs.* photon energy ($h\nu$), (B) Photoluminescence (PL) spectra of $BiVO_4$ and CoAl-MMO/$BiVO_4$ samples, (C) transient photocurrent response for $BiVO_4$ and CoAl-MMO/$BiVO_4$ samples under an applied potential of 0.5 V *vs.* SCE with several on–off cycles of intermittent visible-light irradiation.

Photoluminescence (PL) spectra of semiconductor materials derive from recombination of photo-induced charge carriers. Higher PL intensity means higher recombination rate of

carriers (electrons and holes) and photocatalytic activity becomes correspondingly lower.[29–31] Fig. 3(B) shows PL spectra of $BiVO_4$ and CoAl-MMO/$BiVO_4$ samples with excitation wavelength of 320 nm. The PL emission wavelength of all samples is centered at 423 nm, different from 590 nm reported by R. Tang *et al.* on $BiVO_4$ nanosheets and its complex with graphene.[8] $BiVO_4$ alone has the highest PL intensity, and the PL intensity decreases by different extent with CoAl-MMO loading amount, the least one obtained on sample ratio of 0.3 : 5. It's caused by the electron transfer from $CoAl_2O_4$ conduction band (CB) to $BiVO_4$ CB, and meanwhile holes transfer from $BiVO_4$ valence band (VB) to $CoAl_2O_4$ VB under the potential of band energy difference, namely, band offset.[28,32] The above migration of photogenerated carriers makes electrons and holes spatial separation, and tremendous reduces their recombination probability. Accordingly, photogenerated carriers have longer life time to take part in photocatalytic reactions, and the photocatalytic activity of CoAl-MMO/$BiVO_4$ would be improved upon $BiVO_4$. As a photocatalytic activity test, transient photocurrent responses of the composite electrodes with on–off cycles of intermittent visible-light irradiation are studied, as shown in Fig. 3(C). The anodic photocurrent in $Na_2SO_4$ solution represents photocatalytic water oxidation efficiency of generated holes on surface of sample electrode. Among the catalysts, $BiVO_4$ shows the lowest photocurrent, meaning that the least amount of holes participates in water oxidation, caused by the worst separation efficiency between carriers.[33] With the molar ratio being 0.3 : 5, CoAl-MMO/$BiVO_4$ generates the highest photocurrent density.

To investigate the electronic effect, Mott–Schottky (MS) measurement[34,35] has been performed on $BiVO_4$ and CoAl-MMO/$BiVO_4$ series, as shown in Fig. 4(A). For CoAl-MMO/$BiVO_4$ with molar loading ratio of 0 : 5, 0.1 : 5, 0.3 : 5 and 0.5 : 5, the $V_{fb}$ are −0.54 V, −0.61 V, −0.72 V and −0.64 V *vs.* SCE (equivalent to −0.06 V, −0.13 V, −0.24 V and −0.16 V *vs.* NHE at PH = 0), respectively. It is well known that CB potential ($E_{CB}$) of a n-type semiconductor is 0–0.2 V more negative than $V_{fb}$ and is dependent on carrier concentration and electron effective mass. It can be seen that $E_{CB}$ of the samples are more negative than the standard redox potential of $O_2/{}^{\bullet}O_2^-$ (0.28 V *vs.* NHE). It indicates the photogenerated electrons could react readily with adsorbed $O_2$ to produce ${}^{\bullet}O_2^-$ (ref. 36), and ${}^{\bullet}O_2^-$ is active free radical in desulfurization reactions. Photocatalytic desulfurization activity has been investigated *via* thiophene decomposition, the result shown in Fig. 4(B). The most negative $V_{fb}$ of −0.24 V corresponds to the highest desulfurization efficiency, is obtained with CoAl-MMO/$BiVO_4$ ratio of 0.3 : 5.

In summary, there are three significant merits of CoAl-MMO loading on $BiVO_4$ *via* sintering mixture of CoAl-LDH and $BiVO_4$. Firstly, it exhibits red shift of the whole band edge upon CoAl-MMO loading. That widens and enhances visible light absorption and utilization. Secondly, nanosized n–p heterojunction has been formed between CoAl-MMO particles and $BiVO_4$. It endows carriers' spatial separation, which has been proved by PL intensity decrease. Thirdly, more negative $V_{fb}$ has been obtained (dashed lines in Scheme 1), which benefits formation of ${}^{\bullet}O_2^-$. Interestingly, the above three effects changes along with

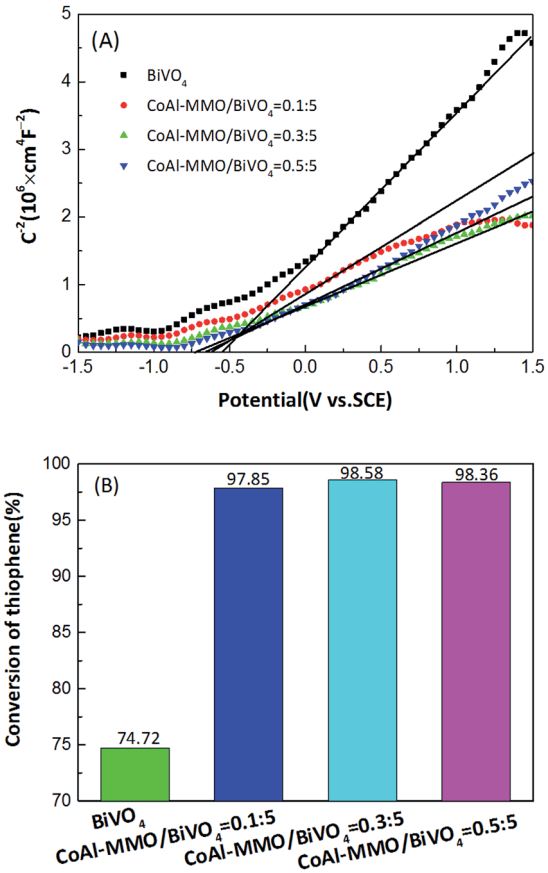


Fig. 4 (A) Mott–Schottky (MS) plots of $BiVO_4$ and CoAl-MMO/$BiVO_4$. (B) Photocatalytic desulfurization of thiophene on $BiVO_4$ and $BiVO_4$ loaded with various ratios of CoAl-MMO (conditions: initial thiophene content: 200 ppm; airflow velocity: 5 mL $min^{-1}$; $H_2O_2$: 0.128 mL; the concentration of photocatalyst: 1 g $L^{-1}$; reaction time: 6 h).

CoAl-MMO loading amount, and 0.3 : 5 is the best in each aspect. Thus, based on the three merits, highly efficient thiophene desulfurization has been realized on CoAl-MMO/$BiVO_4$. Schematic description of the mechanism for thiophene desulfurization on CoAl-MMO/$BiVO_4$ has been shown in Scheme 1. Along with CoAl-MMO loading amount modifying, band gap

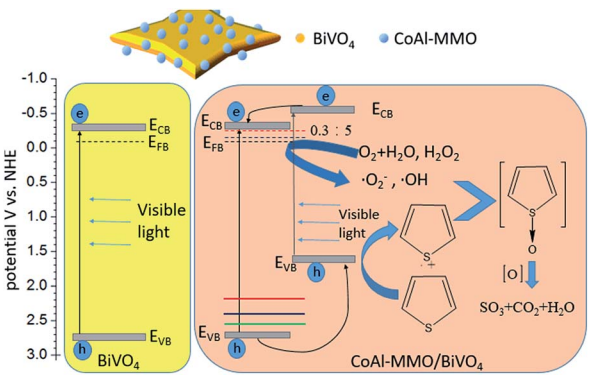


Scheme 1 Schematic description of the mechanism for the photocatalytic oxidation of thiophene on CoAl-MMO/$BiVO_4$.

energy of CoAl-MMO/$BiVO_4$ becomes smaller and more visible light has been absorbed to excite carriers. 3 colored lines above $E_{VB}$ in Scheme 1 indicate that $E_{VB}$ moves upward, corresponding to band gap shortening, caused by changing loading amount of CoAl-MMO. Due to the band offset of heterojunction, photogenerated holes and electrons transfer to CoAl-MMO and $BiVO_4$ respectively (black curved arrows in Scheme 1). Electron on $BiVO_4$ reacts with absorbed $O_2$ to $^{\bullet}O_2^-$. On the other hand, hole on CoAl-MMO reacts with $OH^-$ forming $^{\bullet}OH$, meanwhile some hole is readily captured by thiophene to forming radical cation $C_4H_4S^{\bullet+}$ (blue curved arrows in Scheme 1). Interaction of the active oxygen species ($^{\bullet}O_2^-$ and $^{\bullet}OH$) with the sulfur radical cations ($C_4H_4S^{\bullet+}$) induces a series of oxidation reactions, at last, thiophene has been almost completely oxidized to $SO_3$, $CO_2$, and $H_2O$.[36–38] As a result of the profound effects of CoAl-MMO loading and optimization, the desulfurization efficiency reaches up to 98.58% on 0.3 : 5 CoAl-MMO/$BiVO_4$.

## Conclusions

Four-angle star-like CoAl-MMO/$BiVO_4$ photocatalysts has been synthesized by a hydrothermal method and later sintering. CoAl-MMO loading on $BiVO_4$, dispersed as amorphous particles on its surface, brings advantages to photocatalytic performance from three aspects, such as visible light enhancement, heterojunctions for carrier spatial separation, and making $V_{fb}$ more negative as well. Therefore, photocatalytic desulfurization efficiency by CoAl-MMO/$BiVO_4$ has been improved largely, compared to $BiVO_4$ under visible light irradiation, from under 75% to over 97%. After optimizing the loading amount, 98.58% conversion of thiophene has been achieved with molar loading ratio of 0.3 : 5. This work has demonstrated that CoAl-MMO is not only cost-effective, but also plays a significant role in enhancing the photocatalytic activity of $BiVO_4$. It points that low-cost and effective mixed metal oxide loading on other photocatalysts may be a promising choice in photocatalytic desulfurization.

## Acknowledgements

This study was supported by the National Natural Science Foundation of China (21401093), Program for Liaoning Excellent Talents in University (LNET LR2015036), the Opening Funds of State Key Lab of Chemical Resource Engineering.

## Notes and references

1 V. L. Vopa and C. N. Satterfield, *J. Catal.*, 1988, **110**, 375.
2 A. J. Hernández-Maldonado and R. T. Yang, *J. Am. Chem. Soc.*, 2004, **126**, 992.
3 G. Palmisano, V. Augugliaro, M. Pagliaro and L. Palmisano, *Chem. Commun.*, 2007, **33**, 3425.
4 T. H. T. Vu, T. T. T. Nguyen, P. H. T. Nguyen, M. H. Do, H. T. Au, T. B. Nguyen, D. L. Nguyen and J. S. Park, *Mater. Res. Bull.*, 2012, **47**, 308.
5 A. L. Linsebigler, G. Lu and J. T. Yates, *Chem. Rev.*, 1995, **95**, 735.
6 A. Kudo, K. Omori and H. Kato, *J. Am. Chem. Soc.*, 1999, **121**, 11459.
7 Y. Chen, X. Ma, D. Li, H. Wang and C. Huang, *RSC Adv.*, 2017, **7**, 4395.
8 Z.-R. Tang, Q. Yu and Y.-J. Xu, *RSC Adv.*, 2014, **4**, 58448.
9 S. Liu, Z.-R. Tang, Y. Sun, J. C. Colmenares and Y.-J. Xu, *Chem. Soc. Rev.*, 2015, **44**, 5053.
10 C. Han, N. Zhang and Y.-J. Xu, *Nano Today*, 2016, **11**(3), 351.
11 X. Lin, B. Wei, X. Zhang, M. Song, S. Yu, Z. Gao, H. Zhai, L. Zhao and G. Che, *Sep. Purif. Technol.*, 2016, **169**, 9.
12 X. Lin, D. Xu, J. Zheng, M. Song, G. Che, Y. Wang, Y. Yang, C. Liu, L. Zhao and L. Chang, *J. Alloys Compd.*, 2016, **688**, 891–898.
13 X. Lin, D. Xu, S. Jiang, F. Xie, M. Song, H. Zhai, L. Zhao, G. Che and L. Chang, *Catal. Commun.*, 2017, **89**, 96.
14 X. Lin, D. Xu, Y. Xi, R. Zhao, L. Zhao, M. Song, H. Zhai, G. Che and L. Chang, *Colloids Surf., A*, 2017, **513**, 117.
15 B. Zhang, J. Li, B. Zhang, R. Chong, R. Li, B. Yuan, S. M. Lu and C. Li, *J. Catal.*, 2015, **332**, 95.
16 Q. Yang, F. Chen, X. Li, D. Wang, Y. Zhong and G. Zeng, *RSC Adv.*, 2016, **6**, 60291.
17 F. Lin, D. Wang, Z. Jiang, Y. Ma, J. Li, R. Li and C. Li, *Energy Environ. Sci.*, 2012, **5**, 6400.
18 X. Gao, F. Fu, L. P. Zhang and W. Li, *Phys. B*, 2013, **419**, 80.
19 Y. Tang, R. Wang, Y. Yang, D. Yan and X. Xiang, *ACS Appl. Mater. Interfaces*, 2016, **8**, 19446.
20 J. Zhao, Z. Lu, M. Shao, D. Yan, M. Wei, D. G. Evans and X. Duan, *RSC Adv.*, 2013, **3**, 1045.
21 Z. Yang, Z. Song, G. Chu, X. Kang, T. Ren, W. Yang and Q. Qiao, *J. Mater. Sci.*, 2012, **47**, 4205.
22 A. Walsh, S. H. Wei, Y. Yan, M. M. Al-Jassim, J. A. Turner, M. Woodhouse and B. A. Parkinson, *Phys. Rev. B: Condens. Matter Mater. Phys.*, 2007, **76**, 165119.
23 S. Miyazaki, *J. Vac. Sci. Technol., B*, 2001, **19**, 2212.
24 H. Xu, C. Wu, H. Li, J. Chu, G. Sun, Y. Xu and Y. Yan, *Appl. Surf. Sci.*, 2009, **256**, 597.
25 M. A. Butler, *J. Appl. Phys.*, 1997, **48**, 1914.
26 L. Zhou, W. Wang, S. Liu, L. Zhang, H. Xu and W. Zhu, *J. Mol. Catal. A: Chem.*, 2006, **252**, 120.
27 X. Dang, X. Zhang, X. Dong, W. Ruan, H. Ma and M. Xue, *RSC Adv.*, 2014, **4**, 54655.
28 N. G. Matveeva and A. I. Shelykh, *Phys. Status Solidi B*, 1972, **50**, 83.
29 F. Wang, L. Liang, L. Shi, K. Chen and J. Sun, *Appl. Catal., A*, 2016, **521**, 104.
30 L. Shi, L. Lin, J. Ma and J. Sun, *Superlattices Microstruct.*, 2013, **62**, 128.
31 L. Jing, Y. Qu, B. Wang, S. Li, B. Jiang, L. Yang, W. Fu, H. Fu and J. Sun, *Sol. Energy Mater. Sol. Cells*, 2006, **90**, 1773.
32 T. Fan, C. Chen and Z. Tang, *RSC Adv.*, 2016, **6**, 9994.
33 Z. Zhang, M. Wang, W. Cui and H. Sui, *RSC Adv.*, 2017, **7**, 8167.
34 E. Gao, W. Wang, M. Shang and J. Xu, *Phys. Chem. Chem. Phys.*, 2011, **13**, 2887.

35 F. Cardon and W. P. Gomes, *J. Phys. D: Appl. Phys.*, 1978, **11**, L63.
36 F. Lin, Z. Jiang, N. Tang, C. Zhang, Z. Chen, T. Liu and B. Dong, *Appl. Catal., B*, 2016, **188**, 253.
37 R. M. Mohamed and E. S. Aazam, *Appl. Catal., A*, 2014, **480**, 100.
38 F. Lin, Y. Zhang, L. Wang, Y. Zhang, D. Wang, M. Yang, J. Yang, B. Zhang, Z. Jiang and C. Li, *Appl. Catal., B*, 2012, **127**, 363.